

Brightening and Control of Spin-Forbidden Dark Excitons in a Strained Monolayer Semiconductor

Shuo Du, Feng Jin, Xinbao Liu, Xin Huang, Yang Yang, Haifang Yang, Junjie Li, Qingming Zhang, Sheng Meng, Yang Guo,* and Changzhi Gu*

Dark excitons are fascinating for condensed matter physics, quantum information processing, and optoelectronics due to their long lifetimes. However, direct optical access to dark excitons is still challenging due to the violation of the spin selection rule. Here, a new scheme for the brightening of spin-forbidden dark exciton in WS_2 monolayers by creating artificial out-of-plane shear strain that induces an effective in-plane pseudo-magnetic field is proposed. To reveal dark excitons, low-temperature magneto-photoluminescence experiments on the strained WS_2 monolayers are performed. It is found that the dark excitons appear at 59 meV below the bright ones and exhibit an asymmetric magnetic field dependence, which is in agreement with the model taking into account the effect of the out-of-plane shear strain on spin-flip processes of exciton states. The fieldless scheme has great potential in the application of dark excitons for new quantum information processing devices.

1. Introduction

Since the discovery of atomically thin Van der Waals materials such as graphene and transition metal dichalcogenide monolayers (TMD-MLs), interest in valley physics at energy band extrema in momentum space has been rekindled, due to its potential application on quantum information.^[1–3] In a TMD-ML, the band

S. Du, F. Jin, X. Liu, X. Huang, Y. Yang, H. Yang, J. Li, Q. Zhang, S. Meng, Y. Guo, C. Gu


Beijing National Laboratory for Condensed Matter Physics
Institute of Physics
Chinese Academy of Sciences
Beijing 100190, China

E-mail: yangguo@iphy.ac.cn; czgu@iphy.ac.cn

S. Du, X. Liu, X. Huang, S. Meng, Y. Guo, C. Gu
School of Physical Sciences
CAS Key Laboratory of Vacuum Physics
University of Chinese Academy of Sciences
Beijing 100190, China

X. Liu, J. Li, S. Meng
Songshan Lake Materials Laboratory Dongguan
Guangdong 523808, China

Q. Zhang
School of Physical Science and Technology
Lanzhou University
Lanzhou 730000, China

 The ORCID identification number(s) for the author(s) of this article can be found under <https://doi.org/10.1002/lpor.202300185>

DOI: 10.1002/lpor.202300185

edges are located at the K and K' valleys of the hexagonal Brillouin zone, and the combined action of broken inversion symmetry, time reversal symmetry, and strong spin-orbit coupling (SOC) brings out valley-contrasted spin splitting in both of conduction and valence bands. Similar to spin polarization, valley polarization associated with pseudospin indices could be utilized as a quantum information carrier.^[1,2,4–7] Evidencing this point, valley polarization of TMD-MLs has been extensively studied in the past decade, and the possibility of the spin-allowed bright exciton states as a quantum bit has been demonstrated through optically pumping valley polarization along with generating and detecting valley coherence.^[2,5,6] Despite the progress on manipulating valley

polarization degree, the relatively short radiative lifetime (<1 ns) has prevented the bright excitons of TMD-MLs from a long-lived qubit in quantum devices. In contrast, the recombination time of spin-forbidden dark exciton states composed of electron-hole pairs with parallel spin is several orders of magnitude longer than that of bright ones in TMD-MLs,^[8–10] which make them one of promising candidates to continue the valleytronics version of qubit for quantum information.^[11]

Due to the violation of spin selection rules, however, the dark excitons in TMD-MLs are difficult to be directly accessed optically.^[12,13] According to the former studies, the spin-flip processes are required to induce the radiative decay of dark excitons, and the mechanism of achieving dark exciton optical brightening with conventional far-field optical techniques could be summarized into two types.^[14,15] One mechanism is due to the Rashba spin-orbit coupling that arises whenever the reflection symmetry in the ML plane is broken. A virtual transition in the conduction band attributed to the SOC mixing will facilitate an intrinsic spin flip, inducing an out-of-plane dipole transition that can be effectively excited by an out-of-plane optical field^[8,14,16–22] (Note S1, Supporting Information). Another mechanism of spin-flip is spin mixing of excitons by applying a strong in-plane magnetic field, which induces a weakly allowed in-plane optical transition by the Zeeman effect.^[9,23–26] Using a large field of ≥ 14 T, a radiative decay rate of dark excitons $\Gamma \approx 10^{-3} \Gamma_B$ can be obtained in MoS_2 -MLs with in-plane optical transition,^[26] where Γ_B is the radiative decay rate of the bright excitons. However, these mechanisms usually require a complicated experimental framework

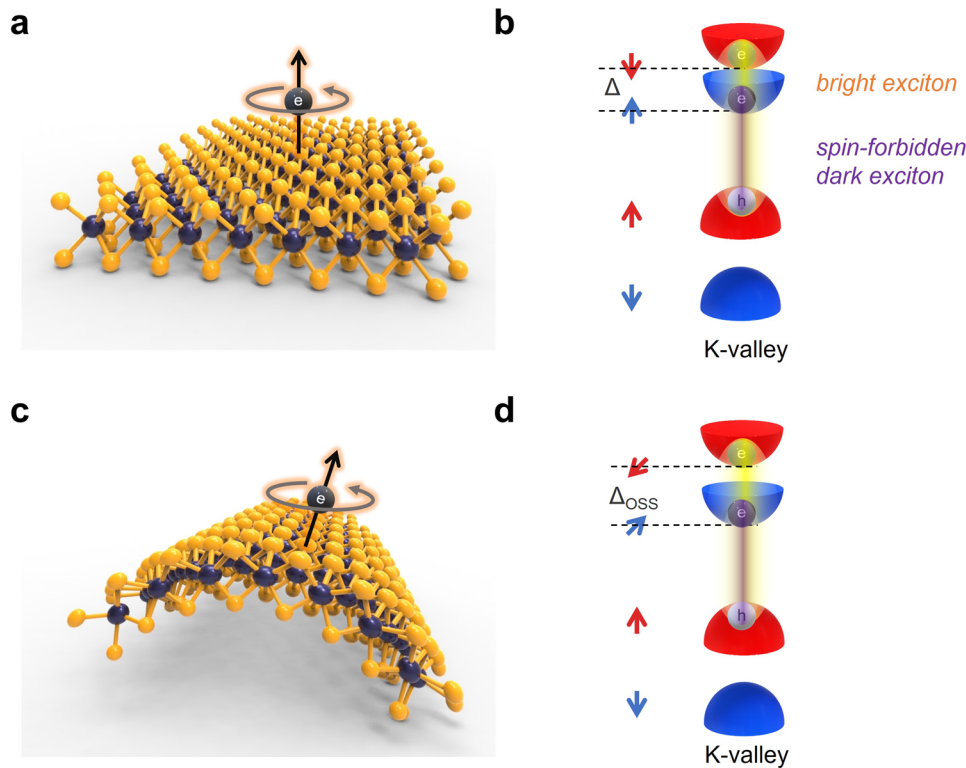


Figure 1. Dark excitons in nonstrained and out-of-plane shear strained WS_2 . a,b) Schematic illustration of the lattice structures and band structure at K valley of nonstrained WS_2 -ML. c,d) Schematic illustration of the lattice structures and band structure at K valley of out-of-plane shear strained WS_2 -ML.

such a strong parallel magnetic field or in-plane light with illumination along a single atomic-layer thick sheet of TMD-MLs. The mechanism and realization method of brightening dark exciton still need to be explored.

Apart from these two approaches, recently, a new one of spin-flip induced with lattice deformation has been theoretically investigated on TMD-MLs,^[27,28] especially the shear deformation which results in a mixing of the orbital structure of the Bloch bands caused by out-of-plane strain structures.^[29] Strain breaks the mirror inversion symmetry of the crystal lattice and introduces spin–lattice coupling, which manifests itself as an effective in-plane magnetic field that couples to spin, or a Rashba-like coupling with a magnitude proportional to the mean curvature of the TMDC lattice.^[30] However, there is still a lack of definite experimental evidences proving strain induced spin-flip in TMD-MLs, let alone the brightening of spin-forbidden dark excitons by strain. In addition, the exploration of strain effect strongly relies on the ability to synthesize nanoscale objects with a targeted geometric shape, while construction of on-demand fictitious gauge fields induced by artificial strain distributions on TMD-MLs within micro- or even nanoscale yet represents a challenge.

Here, we present a new approach for brightening of spin-forbidden dark exciton into WS_2 -MLs by creating artificial out-of-plane shear strain (OSS). To reveal the dark exciton emission, low temperature magneto-photoluminescence experiments are conducted for strained WS_2 -MLs. Our observations show that the dark excitons appear at 59 meV below the bright ones under zero magnetic field, while they become split into two nondegenerate

spin states under nonzero out-of-plane magnetic field and exhibit an asymmetric dependence on it. These results can be well explained by our model taking into account the effect of the OSS on spin-flip processes of exciton states.

2. Results and Discussion

2.1. Spin-flip Mechanism Induced by Strain

Figure 1a,b exhibits schematics of the lattice structure and band structure at the K valley of a WS_2 -ML. Owing to the large spin-splitting in the valence band (VB) compared to the conduction band (CB), the direct band-edge features are characterized by spin-split electron states $|\uparrow\rangle_e$ and $|\downarrow\rangle_e$ with the SOC energy Δ from CB and spin-specific hole state $|\uparrow\rangle_h$ from the highest lying VB at K valley. The corresponding exciton states of unstrained TMD-MLs can be dark with parallel electron and hole spins $|D\rangle = |\uparrow, \uparrow\rangle_{eh}$ and bright with antiparallel spins $|B\rangle = |\downarrow, \uparrow\rangle_{eh}$. Next, we introduce an out-of-plane perturbation by strain into the system (Figure 1c,d), which could mix the spin components of the quantum states of excitons. Focusing the contribution of shear component of strain, the spin-effective Hamiltonian can be described by^[29]

$$H = \begin{bmatrix} E_0 & a\epsilon_{OSS} \\ a\epsilon_{OSS}^* & E_0 + \Delta \end{bmatrix} \quad (1)$$

where E_0 is the lowest exciton energy under no strain and the magnitude of $\epsilon_{OSS} = \epsilon_{xz} \pm i\epsilon_{yz}$ is presumed to remain in the harmonic regime ($\epsilon_{OSS} \ll 1$). The off-diagonal terms within H result

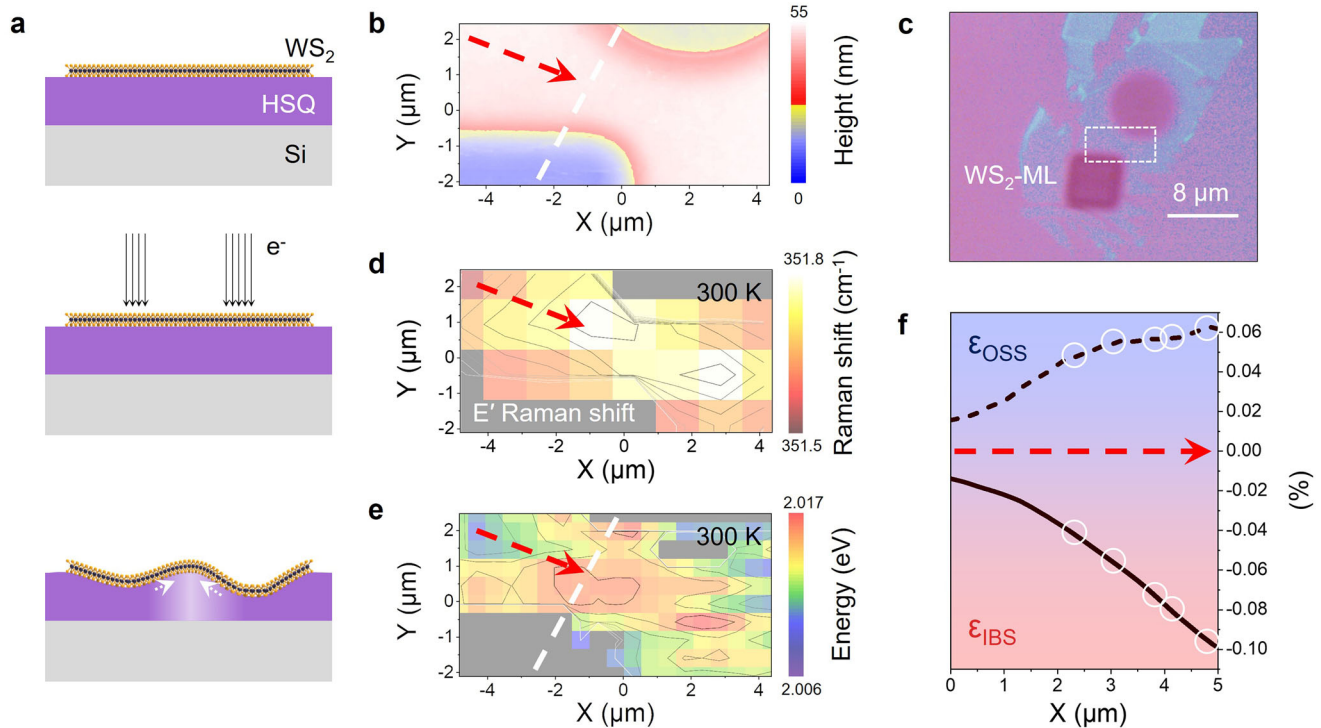


Figure 2. Characterization of strained WS₂-MLs at room temperature. a) Schematic of strain direct writing by using a focused electron beam on a WS₂-ML covering on a HSQ layer. b) AFM topography images of the strained bulge region, the difference between min and max in height is 57 nm. c) Microscopic image of strained WS₂-ML, and the strained bulge region is in the white dashed box. d) Raman peak mapping image of the E' mode of WS₂-ML at room temperature in the strained bulge region. e) PL peak mapping image of WS₂-ML at room temperature in the strained bulge region. f) Simulated OSS and IBS profile along the red dashed arrow in (b)/(d)/(e).

from the spin-orbit coupling between different d orbitals,^[27] representing intravalley strain-spin coupling mechanism, and the strength of the coupling depends on ϵ_{OSS} , which is weighted by the deformation potential a . The eigenvalues of the spin-effective Hamiltonian matrix are given by

$$E_{\pm} \cong E_0 + \frac{\Delta}{2} \pm \frac{1}{2} \sqrt{\Delta^2 + |2a\epsilon_{OSS}|^2} \quad (2)$$

It is clear that the out-of-plane perturbation leads to an anti-crossing of spin-split electron states $|\uparrow\rangle_e$ and $|\downarrow\rangle_e$, and the corresponding energy splitting becomes $\Delta_{OSS} = \sqrt{\Delta^2 + |2a\epsilon_{OSS}|^2}$. From the viewpoint of inversion symmetry breaking, the strain-induced off-diagonal perturbation to spin sub-bands is equivalent to an in-plane magnetic field in terms of its effects on changing the spin characteristics of band-edge states,^[29] and such strain effect can be quantitatively converted into the magnitude of in-plane pseudo-magnetic field $B_{\parallel}(T) \cong \frac{2a}{g\mu_B} \epsilon_{OSS}$, where μ_B is Bohr magneton and g is the transverse electron g-factor.^[31] In addition, the spin mixing states of bright and dark exciton, which correspond to the two eigenvectors of the spin-effective Hamiltonian matrix, can be expressed with noninteraction basis vectors $|D\rangle$ and $|B\rangle$ as

$$|D\rangle_{mix} = c_1^C |D\rangle + c_1^F |B\rangle \quad (3)$$

$$|B\rangle_{mix} = c_2^C |B\rangle + c_2^F |D\rangle \quad (4)$$

where c_n^C and c_n^F ($n = 1, 2$) are spin-conserving and spin-flipping coefficient, respectively, which can be mathematically formulated (Note S2, Supporting Information) as

$$|c_n^F|^2 = \frac{W^2}{1+W^2} \text{ and } |c_n^C|^2 = \frac{1}{1+W^2}, \quad (5)$$

where the out-of-plane spin coupling factor W is equal to $\frac{a|\epsilon_{OSS}|}{\Delta_{OSS}}$. So, it is clear that, with the increase of ϵ_{OSS} , the $|c_n^F|^2$ is close to 0.5, which indicates the OSS-induced brightening of dark excitons.

2.2. Characterization of Strained WS₂-MLs at Room Temperature

To introduce such OSS, our samples of strained WS₂-MLs are prepared as shown in **Figure 2a**. First, an unstrained WS₂-ML is obtained by mechanical exfoliation from a bulk WS₂ crystal and transferred to a silicon substrate covered with a spin-coated 300 nm-thick hydrogen silsesquioxane (HSQ) layer that serves as an electro-sensitive deformable material (Note S3, Supporting Information). And then, a focused electron beam is used to illuminate two adjacent areas without overlap in the WS₂-ML in sequence, giving rise to local collapse of WS₂-ML due to decomposition of HSQ layer beneath it (Note S4, Supporting Information).^[32] As a result, a bulge will appear between two adjacent irradiated areas after the squeezing of these two collapsed ranges, which is attributed to in-plane stress on its both sides

(white dashed arrow). This can contribute to the pure OSS on WS₂-MLs, avoiding other the electron bombardment effect of irradiated areas (Note S5). The atomic force microscopy (AFM) image (Figure 2b) shows that the local area marked with the white square in the microscopic picture (Figure 2c) exhibits the shape of valley-ridge-valley, and the cross-section of height profile along the white dashed line is shown in Figure S7c (Supporting Information). Accordingly, there exist obvious lattice deformation in this local area, which can be observed from the 2D mapping image of Raman shift, as shown in Figure 2d. Compared with an unstrained WS₂-ML (Note S7, Supporting Information), the Raman mode E' becomes softening in the collapsed ranges of the strained WS₂-ML while it becomes stiffening in the central bulge range, which correspond to tensile strain and compressive strain respectively.^[33] In particular, there is a gradient of compressive strain in the bulge along the direction marked by the red dashed line in Figure 2c. Moreover, the exciton emission at the band edge exhibits the matched change with strain, as shown in Figure 2e that is the 2D mapping image of photoluminescence (PL) peak position at room temperature. The red dashed arrow in the Figure 2e tells the direction of compressive strain increase, where the PL peak moves from about 2.009 to 2.017 eV. The typical experimental value for WS₂-ML exciton energy shifts as a function of biaxial strain at room temperature is about ±90 meV %⁻¹,^[30,34] so compared with the PL peak of unstrained WS₂-ML (2.006 eV) in Note S7 (Supporting Information), the maximum compressive strain on the bulge can be calculated as −0.12%. Figure S6 (Supporting Information) shows the profile line of PL peak positions across the shape of valley-bulge-valley marked by the white dashed line in Figure 2e, indicating a sharp strain change from tensile to compressive strain there. Different from in-plane biaxial strain (IBS), there is no general agreement on how to calculate OSS from PL spectra. For this reason, the finite-element method (FEM) is used to calculate the OSS of the bulge region (detailed in Notes S9 and S10, Supporting Information). The simulated results match well with the measured AFM topography and the peaks-shift-calculated IBS in Figure 2b,e, and the simulated OSS along the red dashed arrow is shown in Figure 2f, with the maximum | ϵ_{OSS} | reaching 0.063%. Meanwhile, it also shows that both of the OSS and the compressive IBS increase along the red arrow in the bulge region.

2.3. Low-temperature PL of a Strained WS₂-ML

Temperature can affect the energy distribution and intensity of exciton emission.^[22,35] In order to reduce thermal disturbance and investigate the dark exciton emission of strained WS₂-MLs, a low-temperature PL experiment is conducted at 1.8 K, using the standard geometry configuration where the excitation and detection light propagates perpendicular to the ML plane. Figure 3a shows a set of PL spectra obtained from the bulge in the strained WS₂-ML along the red dashed line in Figure 2c. To be clear, we firstly describe the spectral feature of the unstrained ML (the top panel of Figure 3a). It can be seen that the highest energy peak X⁰ originated from the neutral exciton emission (bright exciton) is located at 2.085 eV and the secondary lower-in-energy peak T contributed from negative trions is at 2.057 eV, followed with a series of low energy peaks labeled Lⁿ ($n = 1, 2, 3, \dots$) that could be

attributed to recombination processes of localized excitons.^[36,37] There is no observation of the dark exciton emission in this spectrum because of the violation of spin selection rules. And the whole PL spectrum can be fitted well with a set of Gaussian functions (see the thick light blue curve for the calculated PL spectrum), which is agreement with the previous studies.

Compared with the unstrained WS₂-ML, the energy peaks X⁰, T, and Lⁿ show strain-dependent blueshifts, and the maximum energy shift of X⁰ is about 17 meV in our observation. In particular, an addition energy peak appears between localized excitons L¹ and L2 and gradually becomes more obvious with the increase of strain, which should be assigned to the dark exciton X^D brightened by OSS as described above. It should be noted that, some of previous studies support that the peak at this position (about 50 meV lower than X⁰) is exactly the neutral dark exciton,^[17,24,26] while others consider this position is the dark trion,^[38,39] so there are controversies over the position of this new peak, but the spin-flip process do contribute to the brightening of both these dark-related-states.^[14,26,38] Each of these strain-dependent PL spectra can be fitted well with a set of Gaussian functions, respectively, as shown in Figure 3a. Figure 3b exhibits the 2D color map of fitting PL intensity of bright (X⁰) and dark exciton (X^D) emissions as a function of the compressive IBS calculated by X⁰ peak shifts (175 meV %⁻¹),^[34] and together with the corresponding OSSs are marked by white circles in Figure 2f. It is clear that the peak intensity of the X⁰ emission becomes decreased while its peak position has an obvious blue shift with the IBS and OSS increasing. In contrast, the peak intensity of the X^D emission becomes increased while its peak position has a slight red shift with the increase of OSS. The minimal energy splitting between X⁰ and X^D excitons is about 59 meV, which is very close to the previous results.^[17,24] And it increases up to 73 meV with the strain increasing, which is mainly contributed to the blue shift of X⁰. The exciton coherence lifetime τ which is connected by $L\tau = \hbar$, with L being the full excitonic linewidth,^[40] so the full-width at half-maximum (FWHM) of PL peaks can be used to roughly compare the lifetime of excitons, that is, the narrower the line width, the longer the lifetime. The FWHM of maximum strained WS₂ X⁰ is 25 meV, while that of X^D is 19 meV. The lifetime of dark excitons is longer than the bright ones. The additional evidence for assigning this new energy peak X^D to spin-forbidden dark excitons is the ratio between the PL intensity of X^D and X⁰, which should follow a simple quadratic law: X^D/X^B intensity ratio $\approx |\epsilon_{OSS}|^2$ according to Equation (5). In Figure 3c, we present the ratio between the PL intensity of X^D and X⁰ emissions as a function of OSS. The measured quadratic behavior (the black parabola fitting curve) is a strong indication that this new energy peak X^D corresponds to the recombination of the dark excitons which have been brightened by artificial strain in the WS₂-ML.

2.4. Magneto-PL of a Strained WS₂-ML at 1.8 K

In next, we further demonstrate that our observation is originated from dark excitons by investigating the symmetry-dependent fine structure of dark excitons of the TMD-MLs. At the equilibrium state, the WS₂-ML belongs to the symmetry group D_{3h}, with W and S atoms arranged in a hexagonal lattice.^[41] According to the previous studies, the bright excitons correspond to the Γ_6 ($\uparrow\downarrow, \downarrow\uparrow$)

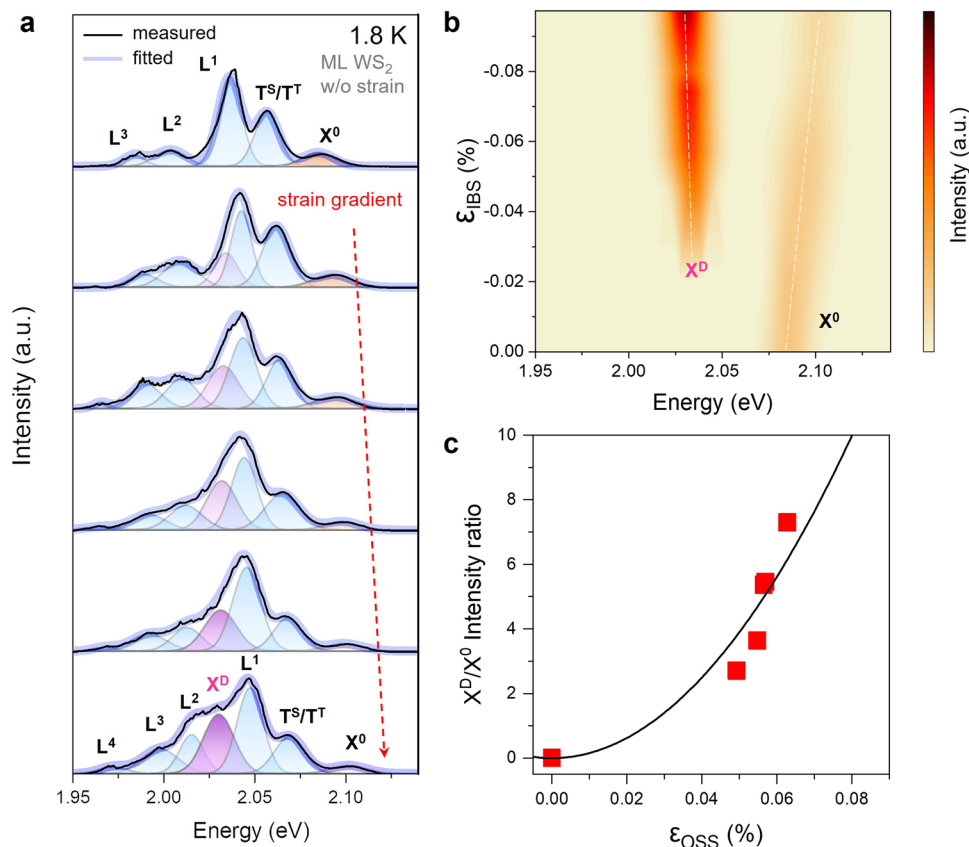


Figure 3. Dark excitons in nonstrained and out-of-plane shear strained WS_2 . Low-temperature PL of a strained WS_2 -ML. a) Waterfall plot of low-temperature PL spectra of WS_2 -ML at 1.8 K with the increasing of the strain along the red dashed line in Figure 2. b) Fitting PL intensity of bright (X^0) and dark exciton (X^D) emissions as a function of the IBS. The corresponding OSS can be readout by Figure 2f. c) Ratio between the PL intensity of X^D and X^0 emissions as a function of OSS.

irreducible representation, while the dark excitons can be considered as two irreducible representations Γ_3 ($\uparrow\uparrow - \downarrow\downarrow$) and Γ_4 ($\uparrow\uparrow + \downarrow\downarrow$) of a D_{3h} group.^[24,42] The schematic diagram of excitonic bands with such symmetry-dependent fine structure is displayed in Figure 4b. On the base of the SOC energy splitting Δ_{OSS} , the exciton exchange interaction induces a new energy splitting δ_0 between Γ_3 and Γ_4 dark excitons,^[42] but it usually is too small to be observed (<1 meV for WS_2 -MLs). In fact, it could become larger under a high out-of-plane magnetic field due to Zeeman effect, which make it possible to observe the fine structure of dark excitons by magneto-PL emission.^[24,42]

Our magneto-PL measurement is carried out for the WS_2 -MLs at 1.8K by using the Faraday configuration (applying the out-of-plane magnetic field, detailed in Note S11, Supporting Information). For comparison, we first present the magneto-PL spectra of unstrained WS_2 -MLs as shown in Figure 4a. It can be seen that the PL emission of the unstrained WS_2 -ML is weakly dependent on the magnetic field, and the lifting of the valley degeneracy of X^0 (valley Zeeman effect) with the magnetic field is not apparent under B_{\perp} from 0 to 9 T, which is consistent with the previous results.^[43] In contrast, applying a longitudinal magnetic field B_{\parallel} on the strained WS_2 -ML will lead to an obvious change of PL emission from dark excitons. In Figure 4c, we present 2D color map of PL intensity as a function of B_{\perp} . It can be found that the

PL emission from X^D becomes stronger and wider with increasing B from 0 to 9 T, which may be attributed from the increasing splitting energy (δ) between Γ_3 and Γ_4 dark excitons. By fitting the PL emission from the strain-induced dark excitons at B = 9 T with two Gaussian functions, we can approximately determine the maximum of δ to be 13 meV in our observation. This result is qualitatively consistent with the above discussion, but the value of δ is too larger than the theoretical value calculated by using the formula of Zeeman splitting energy $\delta = \sqrt{\delta_0^2 + (\mu_B g_D B_{\perp})^2}$, where g_D is the dark exciton g-factor. Thus, the total splitting energy (Γ_3, Γ_4) Δ_{total} can be modified as

$$\Delta_{total} = \Delta_{OSS} + \frac{1}{2}\Delta_{exch} = \sqrt{\Delta^2 + |2a\epsilon_{OSS}|^2} + \sqrt{\delta_0^2 + (\mu_B g_D B_{\perp})^2} \quad (6)$$

This means that, in addition to the external magnetic B_{\perp} , there are other factors acting for the coupling of Γ_3 and Γ_4 dark excitons. To examine it, we measure the magneto-PL spectra of strained WS_2 -MLs with a reverse magnetic field $-B_{\perp}$ again. Figure 4d shows the 2D color map of PL intensity as a function of $-B_{\perp}$. Interestingly, the PL emission from dark excitons become suppressed with increasing the reverse magnetic field

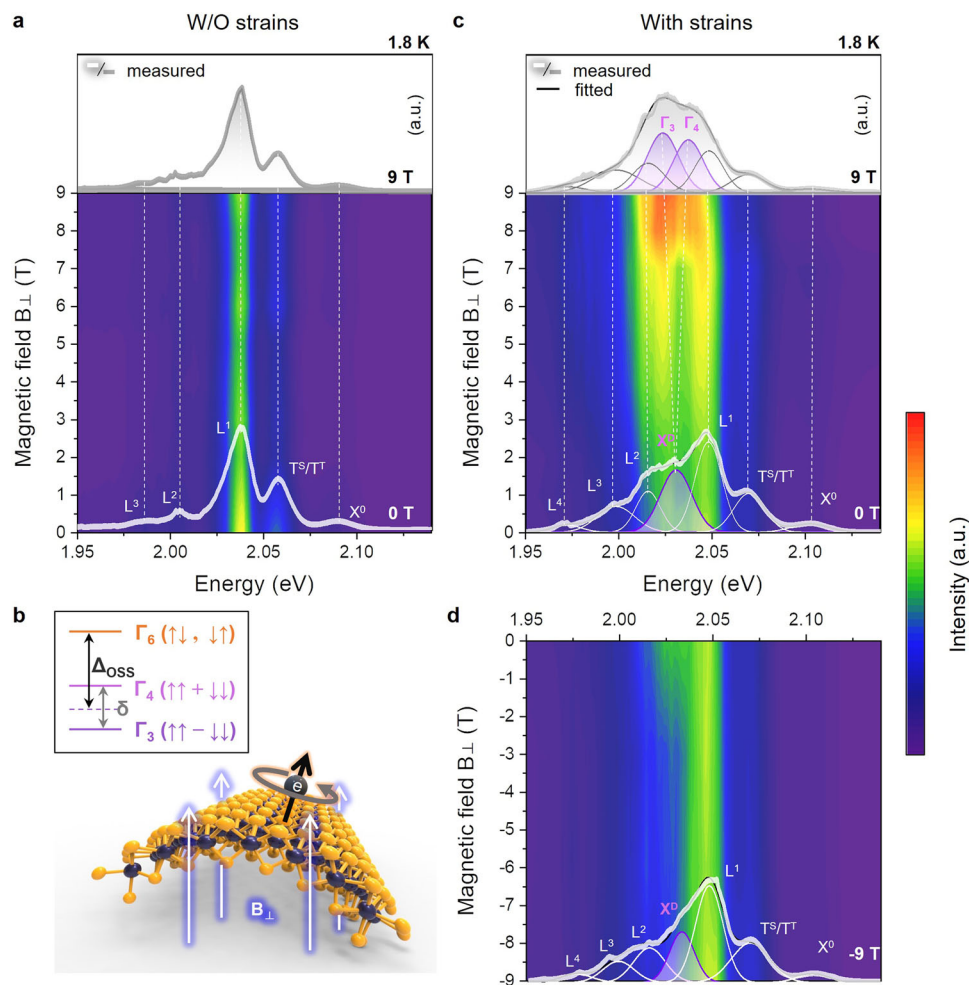


Figure 4. Magneto-photoluminescence of a strained WS_2 -ML at 1.8 K. a) Color map of the variation of the PL intensity as a function of B_{\perp} (0–9 T) of nonstrained WS_2 -ML. b) Sketch of the exciton fine structure and the schematic illustration of the strain lattice structures under B_{\perp} . c) Color map of the variation of the PL intensity as a function of B_{\perp} (0–9 T) of strained WS_2 -ML. d) Color map of the variation of the PL intensity as a function of B_{\perp} (0 to –9 T) of strained WS_2 -ML.

ranging from 0 T to –9 T, which indicates an asymmetric magnetic field dependent behavior. One of possible explanations for this result is to assume that the equivalent magnetic field induced by strain is not in-plane but tilted, which could be resulted from the IBS-induced out-of-plane pseudo-magnetic fields that have been widely reported in graphene and TMDs.^[44–46] The external reverse magnetic field will offset the longitudinal component of the effective magnetic field induced by strain, weakening the coupling of Γ_3 and Γ_4 dark excitons. This asymmetric magnetic field response can be further exploited for new types of magnetic field sensor or magnetometer.

3. Conclusion

In summary, we present a new proposal of brightening of spin-forbidden dark excitons by creating artificial OSS. We theoretically illuminate that the OSS perturbation acting on spin exciton subbands is equivalent to in-plane pseudo-magnetic fields, which resulting in the mixing of bright and dark states by spin-flip processes. By using a low temperature magneto-photoluminescence

spectroscopy, we find that the dark excitons appear at the range of 59–73 meV below the bright ones under zero magnetic field, while they become split into two nondegenerate spin states under nonzero magnetic field and exhibit an asymmetric dependence on the magnetic field. These results are in agreement with the model of strain induced spin-flip processes of exciton states. Our study would provide a fieldless way to manipulate and readout spin-forbidden dark excitons by strain engineering, holding great potential in the application of dark excitons of 2D semiconductors for new quantum information processing devices.

4. Experimental Section

WS_2 Monolayer Preparation: In a typical mechanical exfoliation process, ML of WS_2 was mechanically exfoliated from bulk crystals (HQ Graphene) by using adhesive Scotch tapes, as shown in Figure S2a,b (Supporting Information). By a dry stamping technique,^[17] the flat WS_2 ML on Scotch tape were brought into contact with a target substrate, which is a spin-coated high-purity semiconductor-grade hydrogen silsesquioxane

(HSQ) layer (300 nm) on a silicon substrate, as shown in Figure S2c (Supporting Information).

Strain Patterning: The strained structures in ML WS₂ were directly patterned by using electron beam lithography (EBL, Raith 150),^[32] see Figure S2d (Supporting Information). Here, the electron accelerating voltage is 10 kV, the aperture for adjustment of an electron beam is 20 μm, the working distance is 5 mm, and the write field was selected as 100 μm.

Magneto-PL measurements: The magneto-PL spectroscopy measurements at 1.8 K were performed with a backscattering configuration using a Jobin Yvon HR-Evolution system and a CW laser of 532 nm. The linearly polarized light was used for excitation. The excitation laser power was kept at a level of 10 μW to avoid overheating. The samples were placed in an at-toDRY 2100 cryostat utilizing He as the exchange gas, allowing the sample to be cooled to 1.8 K.

Supporting Information

Supporting Information is available from the Wiley Online Library or from the author.

Acknowledgements

The authors thank Dr. Shengjie Zhang for helpful discussions and the Synergetic Extreme Condition User Facility (SECUF) for experiments. This work was supported by the National Natural Science Foundation of China under Grants Nos. 92265110, 62174179, 61888102, 11974386, 61905274, 12074420, U21A20140, 62071291, 62204259, 62175253, 12025407, 12104491, 11934003, U1932215, and 12274186; the National Key Research Program of China under Grant Nos. 2021YFA1400700, 2021YFA1400200, and 2022YFA1402704; Strategic Priority Research Program of the Chinese Academy of Sciences under Grant Nos. XDB33020200, XDB33000000, XDB28000000, XDB330301, QYZDJ-SSW-SLH042, and XDB33010100; the Key Research Program of Frontier Sciences of CAS under Grant Nos. QYZDJSSWSLH042 and XDPB22; the Beijing Municipal Science & Technology Commission, Administrative Commission of Zhongguancun Science Park under Grant No. Z211100004821009; and the Project for Young Scientists in Basic Research of CAS under Grant No. YSBR021.

Conflict of Interest

The authors declare no conflicts of interest.

Author Contributions

S.D., F.J., and X.L. contributed equally to this work. C.G. and Y.G. supervised the project. Y.G. and S.D. conceived the idea. Y.G., S.M., X.L., S.D., and X.H. did the theoretical analysis and carried out the numerical simulations. S.D., H.Y., and J.L. prepared and fabricated the sample. S.D., F.J., Y.G., Y.Y., and X.Z. performed the magneto-photoluminescence experiments. S.D. and Y.G. did the data analysis and wrote the manuscript. All authors contributed to the revision and discussion of the paper. All authors have given approval to the final version of the manuscript.

Data Availability Statement

The data that support the findings of this study are available from the corresponding author upon reasonable request.

Keywords

pseudo-magnetic field, spin-flip, spin-forbidden dark excitons

Received: February 24, 2023

Revised: May 30, 2023

Published online:

- [1] K. F. Mak, K. He, J. Shan, T. F. Heinz, *Nat. Nanotechnol.* **2012**, *7*, 494.
- [2] K. F. Mak, D. Xiao, J. Shan, *Nat. Photonics* **2018**, *12*, 451.
- [3] X. Liu, M. C. Hersam, *Nat. Rev. Mater.* **2019**, *4*, 669.
- [4] Z. Ye, D. Sun, T. F. Heinz, *Nat. Phys.* **2016**, *13*, 26.
- [5] K. Hao, G. Moody, F. Wu, C. K. Dass, L. Xu, C.-H. Chen, L. Sun, M.-Y. Li, L.-J. Li, A. H. MacDonald, X. Li, *Nat. Phys.* **2016**, *12*, 677.
- [6] H. Zeng, J. Dai, W. Yao, D. Xiao, X. Cui, *Nat. Nanotechnol.* **2012**, *7*, 490.
- [7] A. M. Jones, H. Yu, N. J. Ghimire, S. Wu, G. Aivazian, J. S. Ross, B. Zhao, J. Yan, D. G. Mandrus, D. Xiao, W. Yao, X. Xu, *Nat. Nanotechnol.* **2013**, *8*, 634.
- [8] K. D. Park, T. Jiang, G. Clark, X. Xu, M. B. Raschke, *Nat. Nanotechnol.* **2018**, *13*, 59.
- [9] X. X. Zhang, T. Cao, Z. Lu, Y. C. Lin, F. Zhang, Y. Wang, Z. Li, J. C. Hone, J. A. Robinson, D. Smirnov, S. G. Louie, T. F. Heinz, *Nat. Nanotechnol.* **2017**, *12*, 883.
- [10] Y. Tang, K. F. Mak, J. Shan, *Nat. Commun.* **2019**, *10*, 4047.
- [11] M. D. Eisaman, J. Fan, A. Migdall, S. V. Polyakov, *APL Photonics* **2011**, *82*, 071101.
- [12] G. H. Peng, P. Y. Lo, W. H. Li, Y. C. Huang, Y. H. Chen, C. H. Lee, C. K. Yang, S. J. Cheng, *Nano Lett.* **2019**, *19*, 2299.
- [13] M. Feierabend, S. Brem, A. Ekman, E. Malic, *2D Mater.* **2020**, *8*, 015013.
- [14] A. O. Slobodeniuk, D. M. Basko, *2D Mater.* **2016**, *3*, 035009.
- [15] Z. Li, T. Wang, S. Miao, Z. Lian, S.-F. Shi, *Nanophotonics* **2020**, *9*, 1811.
- [16] M. Rahaman, O. Selyshchev, Y. Pan, R. Schwartz, I. Milekhin, A. Sharma, G. Salvan, S. Gemming, T. Korn, D. R. T. Zahn, *Adv. Opt. Mater.* **2021**, *9*, 2101801.
- [17] G. Wang, C. Robert, M. M. Glazov, F. Cadiz, E. Courtade, T. Amand, D. Lagarde, T. Taniguchi, K. Watanabe, B. Urbaszek, X. Marie, *Phys. Rev. Lett.* **2017**, *119*, 047401.
- [18] T. W. Lo, X. Chen, Z. Zhang, Q. Zhang, C. W. Leung, A. V. Zayats, D. Lei, *Nano Lett.* **2022**, *22*, 1915.
- [19] R. J. Gelly, D. Renaud, X. Liao, B. Pingault, S. Bogdanovic, G. Scuri, K. Watanabe, T. Taniguchi, B. Urbaszek, H. Park, M. Loncar, *Nat. Commun.* **2022**, *13*, 232.
- [20] Y. Zhou, G. Scuri, D. S. Wild, A. A. High, A. Dibos, L. A. Jauregui, C. Shu, K. De Greve, K. Pistunova, A. Y. Joe, T. Taniguchi, K. Watanabe, P. Kim, M. D. Lukin, H. Park, *Nat. Nanotechnol.* **2017**, *12*, 856.
- [21] X. Ma, K. Kudtarkar, Y. Chen, P. Cunha, Y. Ma, K. Watanabe, T. Taniguchi, X. Qian, M. C. Hipwell, Z. J. Wong, S. Lan, *Nat. Commun.* **2022**, *13*, 6916.
- [22] T. W. Lo, Q. Zhang, M. Qiu, X. Guo, Y. Meng, Y. Zhu, J. J. Xiao, W. Jin, C. W. Leung, D. Lei, *ACS Photonics* **2019**, *6*, 411.
- [23] Z. Lu, D. Rhodes, Z. Li, D. Van Tuan, Y. Jiang, J. Ludwig, Z. Jiang, Z. Lian, S.-F. Shi, J. Hone, H. Dery, D. Smirnov, *2D Mater.* **2019**, *7*, 015017.
- [24] C. Robert, B. Han, P. Kapuscinski, A. Delhomme, C. Faugeras, T. Amand, M. R. Molas, M. Bartos, K. Watanabe, T. Taniguchi, B. Urbaszek, M. Potemski, X. Marie, *Nat. Commun.* **2020**, *11*, 4037.
- [25] F. Qu, H. Bragança, R. Vasconcelos, F. Liu, S. J. Xie, H. Zeng, *2D Mater.* **2019**, *6*, 045014.
- [26] M. R. Molas, C. Faugeras, A. O. Slobodeniuk, K. Nogajewski, M. Bartos, D. M. Basko, M. Potemski, *2D Mater.* **2017**, *4*, 021003.
- [27] Y. Song, H. Dery, *Phys. Rev. Lett.* **2013**, *111*, 026601.
- [28] A. J. Pearce, E. Mariani, G. Burkard, *Phys. Rev. B* **2016**, *94*, 155416.
- [29] H.-Y. Hwang, S. Lee, Y.-H. Kim, F. Ullah, C. T. Le, Y. S. Kim, K.-J. Yee, C. J. Stanton, Y.-D. Jho, *2D Mater.* **2021**, *9*, 015011.
- [30] Z. Peng, X. Chen, Y. Fan, D. J. Srolovitz, D. Lei, *Light: Sci. Appl.* **2020**, *9*, 190.
- [31] M. R. Molas, A. O. Slobodeniuk, T. Kazimierzczuk, K. Nogajewski, M. Bartos, P. Kapuscinski, K. Oreszczuk, K. Watanabe, T. Taniguchi, C.

- Faugeras, P. Kossacki, D. M. Basko, M. Potemski, *Phys. Rev. Lett.* **2019**, *123*, 096803.
- [32] S. Du, Y. Guo, X. Huang, C. Sun, Z. Zhang, L. Hu, R. Zheng, Q. Bai, A. Jin, H. Yang, Y. Zhang, J. Li, C. Gu, *Appl. Phys. Lett.* **2022**, *120*, 093104.
- [33] Q. Zhang, Z. Chang, G. Xu, Z. Wang, Y. Zhang, Z. Q. Xu, S. Chen, Q. Bao, J. Z. Liu, Y. W. Mai, W. Duan, M. S. Fuhrer, C. Zheng, *Adv. Funct. Mater.* **2016**, *26*, 8707.
- [34] S. B. Chand, J. M. Woods, E. Mejia, T. Taniguchi, K. Watanabe, G. Grosso, *Nano Lett.* **2022**, *22*, 3087.
- [35] C. T. Yip, T. W. Lo, S.-C. Zhu, G. Y. Jia, H. Sun, C.-H. Lam, D. Lei, *Nanoscale Horiz.* **2019**, *4*, 969.
- [36] D. Vaclavkova, J. Wyzula, K. Nogajewski, M. Bartos, A. O. Slobodeniuk, C. Faugeras, M. Potemski, M. R. Molas, *Nanotechnology* **2018**, *29*, 325705.
- [37] G. Plechinger, P. Nagler, A. Arora, R. Schmidt, A. Chernikov, A. G. Del Aguila, P. C. Christianen, R. Bratschitsch, C. Schuller, T. Korn, *Nat. Commun.* **2016**, *7*, 12715.
- [38] M. Zinkiewicz, A. O. Slobodeniuk, T. Kazimierczuk, P. Kapuscinski, K. Oreszczuk, M. Grzeszczyk, M. Bartos, K. Nogajewski, K. Watanabe, T. Taniguchi, C. Faugeras, P. Kossacki, M. Potemski, A. Babinski, M. R. Molas, *Nanoscale* **2020**, *12*, 18153.
- [39] M. Zinkiewicz, T. Wozniak, T. Kazimierczuk, P. Kapuscinski, K. Oreszczuk, M. Grzeszczyk, M. Bartos, K. Nogajewski, K. Watanabe, T. Taniguchi, C. Faugeras, P. Kossacki, M. Potemski, A. Babinski, M. R. Molas, *Nano Lett.* **2021**, *21*, 2519.
- [40] M. Selig, G. Berghauser, A. Raja, P. Nagler, C. Schuller, T. F. Heinz, T. Korn, A. Chernikov, E. Malic, A. Knorr, *Nat. Commun.* **2016**, *7*, 13279.
- [41] D. Muoi, N. N. Hieu, H. T. T. Phung, H. V. Phuc, B. Amin, B. D. Hoi, N. V. Hieu, L. C. Nhan, C. V. Nguyen, P. T. T. Le, *Chem. Phys.* **2019**, *519*, 69.
- [42] C. Robert, T. Amand, F. Cadiz, D. Lagarde, E. Courtade, M. Manca, T. Taniguchi, K. Watanabe, B. Urbaszek, Marie X., *Phys. Rev. B* **2017**, *96*, 155423.
- [43] M. Koperski, M. R. Molas, A. Arora, K. Nogajewski, M. Bartos, J. Wyzula, D. Vaclavkova, P. Kossacki, M. Potemski, *2D Mater.* **2018**, *6*, 015001.
- [44] D. H. Kang, H. Sun, M. Luo, K. Lu, M. Chen, Y. Kim, Y. Jung, X. Gao, S. J. Parluhan, J. Ge, S. W. Koh, D. Giovanni, T. C. Sum, Q. J. Wang, H. Li, D. Nam, *Nat. Commun.* **2021**, *12*, 5087.
- [45] F. Guinea, M. I. Katsnelson, A. K. Geim, *Nat. Phys.* **2009**, *6*, 30.
- [46] M. A. Cazalilla, H. Ochoa, F. Guinea, *Phys. Rev. Lett.* **2014**, *113*, 077201.